Radiation Measurements 155 (2022) 106788

Contents lists available at ScienceDirect

Radiation Measurements

journal homepage: www.elsevier.com/locate/radmeas

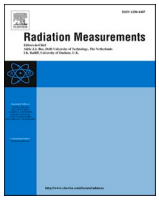

Testing the potential of using fine quartz for dating loess in South Island, New Zealand

A. Avram [a,b], Z. Kabacińska [b], A. Micallef [c,d], A. Timar-Gabor [a,b,*]

[a] Faculty of Environmental Science and Engineering, Babes-Bolyai University, Cluj-Napoca, Romania
[b] Interdisciplinary Research Institute on Bio-Nano-Sciences, Environmental Radioactivity and Nuclear Dating Centre, Babes-Bolyai University, Cluj-Napoca, Romania
[c] Helmholtz Centre for Ocean Research, GEOMAR, Kiel, Germany
[d] Marine Geology & Seafloor Surveying, Department of Geosciences, University of Malta, Malta

ARTICLE INFO

Keywords:
Quartz
Polymineral fine grains
Luminescence
Electron spin resonance
New Zealand loess

ABSTRACT

The applicability of optically stimulated luminescence (OSL) dating on quartz from South Island, New Zealand is hampered by the poor behaviour of the targeted signals. However, most OSL dating studies have been focused on using coarse quartz fractions. Since a previous study conducted from a nearby site demonstrated that coarse quartz (63–90, 90–125, 125–180 and 180–250 μm) is not suitable for OSL dating, we attempt using fine quartz here. Therefore, the standard SAR protocol was applied on 4–11 μm quartz extracted from a loess/paleosol section. Unlike the coarser fractions, the OSL signal of fine quartz displayed satisfactory characteristics which allowed estimating ages ranging from 0.3 ± 0.04 ka to 16 ± 1 ka. In order to understand the differences between the two quartz fractions, we characterise fine (4–11 μm) as well as the usually used coarser grain sizes (> 63 μm) of quartz by electron spin resonance (ESR). No significant differences are reported in qualitative terms between the grain sizes investigated and calibration quartz. We report a higher abundance of intrinsic defects in the fine grain fraction; however, this is typical for quartz from other regions as well, that was amenable for OSL dating. As such, the differences between the fine quartz fraction and the coarse fraction is not yet understood. In addition, two elevated temperature post-infrared infrared protocols ($pIRIR_{225}$ and $pIRIR_{290}$) were applied and polymineral grains extracted from the same samples. Despite residual dose corrections being performed using a modern analogue, pIRIR ages overestimate quartz ages by 19–122% in the case of the application of the $pIRIR_{225}$ protocol and by 25–217% in the case of the application of the $pIRIR_{290}$ protocol. The effect could not be circumvented by the application of a test dose with a magnitude of 50% of the equivalent dose in the $pIRIR_{290}$ protocol. In the case of the application of $pIRIR_{290}$ protocol, dose recovery tests ratios vary from 1.07 ± 0.06 to 1.23 ± 0.05. While not ideal, these results cannot fully explain the differences reported between the ages obtained by fine quartz OSL and the polymineral fine grains pIRIR methods.

1. Introduction

Loess deposits of New Zealand are considered important archives for paleoclimate reconstruction of the southern hemisphere (Alloway et al., 2007), thus recent studies have been centred in establishing high-resolution chronologies.

Optically Stimulated Luminescence Dating (OSL) represents one of the most used dating techniques for Quaternary climate reconstruction. Its applicability has been successful for loess deposits located over both northern and southern hemispheres, respectively (Roberts 2008, 2015). However, since luminescence dating has been perceived to be challenging for loess sediments from South Island of New Zealand, few OSL studies have been reported so far (e.g., Holdaway et al., 2002; Rowan et al., 2012; Sohbati et al., 2016; Micallef et al., 2021; Brezeanu et al., 2021). Even though quartz is considered the preferred dosimeter when young sediments have to be dated due to the higher bleachability of the signal, it is well known that South Island quartz suffers from major problems that restrain its application, namely the weak sensitivity of the signal, with the signal originating from many dim grains and the poor behaviour exhibited in the single aliquot regenerative dose (SAR) protocol (Preusser et al., 2006). These issues have been attributed by the aforementioned study to the short sedimentation history of the mineral grains, as it was reported that quartz sensitisation can be achieved by repeated irradiation/bleaching cycles. A recent study by Brezeanu et al.

* Corresponding author. Faculty of Environmental Science and Engineering, Babes-Bolyai University, Cluj-Napoca, Romania.
E-mail address: alida.timar@ubbcluj.ro (A. Timar-Gabor).

https://doi.org/10.1016/j.radmeas.2022.106788
Received 22 November 2021; Received in revised form 23 March 2022; Accepted 13 May 2022
Available online 17 May 2022

(2021) confirmed that the OSL signals of coarse (>63 μm) quartz displayed low-sensitivity and a significant sensitivity-changes during the repeated SAR cycles. Despite these limitations, there are few OSL studies that reported ages on quartz in New Zealand (e.g., Holdaway et al., 2002; Nichol et al., 2003; Rowan et al., 2012; Hornblow et al., 2014; Sohbati et al., 2016). Holdaway et al. (2002) reported luminescence ages on 90–125 μm quartz that were in agreement with ^{14}C ages for colluvial sediments from Otago, South Island of New Zealand. Later, Rowan et al. (2012) have successfully obtained a luminescence chronology for glaciofluvial sediments from Canterbury Plains of South Island using 180–211 μm quartz. Moreover, a more recent study conducted by Sohbati et al. (2016) reported a good agreement between 40 and 63 μm quartz SAR-OSL and $pIRIR_{290}$ luminescence ages in the attempt to refine palaeorockfall chronologies in New Zealand using luminescence dating.

Since the applicability of luminescence dating on quartz grains extracted from New Zealand sediments is not always a viable solution, other luminescence studies conducted on South Island considered that using infrared stimulated luminescence (IRSL) signal on coarse K-rich feldspars (Preusser et al., 2005) or on polymineral fine grains (e.g., Berger et al., 2001, 2002; Hormes et al., 2003; Rother et al., 2009; Almond et al., 2001, 2007; Shulmeister et al., 2010) is a more appropriate solution for obtaining luminescence chronologies. It is well known that the IRSL signal of feldspars suffers from anomalous fading and thus recent studies have developed measurement protocols that are able to circumvent fading. Such protocols consist of a double IR stimulation and they are known as post infrared-infrared stimulated luminescence protocols, $pIRIR_{225}$ and $pIRIR_{290}$. Even though, these pIRIR protocols have been successfully applied on coarse K-feldspars as well as on polymineral fine grains extracted from loess deposits all over the world (e.g., Roberts 2008; Buylaert et al., 2009, 2011; Thiel et al., 2011; Vasiliniuc et al., 2012; Yi et al., 2016; Bösken et al., 2017; Zhang et al., 2018; Veres et al., 2018; Avram et al., 2020; Avram et al., 2022), their potential has not been fully explored for New Zealand sediments. Only three dating studies have reported $pIRIR_{290}$ luminescence ages (Sohbati et al., 2016; Micallef et al., 2021; Brezeanu et al., 2021) and two studies presented $pIRIR_{225}$ (Micallef et al., 2021; Brezeanu et al., 2021) chronologies on loess extracted from South Island of New Zealand.

To our knowledge, all quartz luminescence ages reported so far in literature were determined using coarse grains quartz (>63 μm), in this study we attempt for the first time to apply SAR-OSL protocol on fine (4–11 μm) quartz extracted from loess in the Canterbury Plains of South Island, New Zealand. $pIRIR_{225}$ as well as $pIRIR_{290}$ protocols have been applied on polymineral fine grains extracted from the same samples.

2. Site description

The foothills of the Southern Alps as well as the lowlands of the Canterbury Plains represent the regions with the widest distribution of loess deposits in South Island of New Zealand (Yates et al., 2018).

The investigated site (44.014973 °S, 171.891569 °E) is located on the southern part of the Canterbury Plains and the eastern side of the South Island of New Zealand. Three modern rivers namely Rakaia, Rangitata and Ashburton flow perpendicularly to the eastern coastal cliff in the Canterbury Plains, discharging into the Pacific Ocean. The loess section is situated less than 1 km away (Fig. S1) from the site investigated by Brezeanu et al. (2021) and therefore a more detailed description of the area can be found in their study.

Luminescence investigations have been performed on seven samples collected at a resolution of 20 cm. The uppermost sample, NZ 6 was collected from a depth of 10 cm while the last sample NZ 12 was collected at a depth of 130 cm.

ESR analysis presented in this study have been performed on sample NZ3 as various grain sizes were available from that specific sample, collected from the loess profile investigated by Brezeanu et al. (2021).

3. Methodology

3.1. Sample preparation

Stainless steel tubes were used for collecting the luminescence sample. The minerals of interest were extracted under subdued red light laboratory conditions. The material from the end of each tube was removed and used for gamma spectrometry measurements. The material from the inner part of the tube was used for 4–11 μm quartz and polymineral grains extraction. In the first step of sample preparation the calcium carbonates and the organic matter were removed by employing a treatment with hydrochloric acid (10% concentration) and hydrogen peroxide (10% concentration followed by 30%). Minerals with diameters smaller than 63 μm were separated by wet sieving. The fine (4–11 μm) polymineral mixture was obtained after Stoke's law settling followed by centrifugation in distilled water (Frechen et al., 1996; Lang et al., 1996). A 10 days treatment with hexafluorosilicic acid was employed in order to isolate the fine (4–11 μm) quartz fraction from the polymineral combination. The extraction procedure for quartz fractions larger than 63 μm (63–90 μm, 90–125 μm, 125–180 μm, 180–250 μm) is described in Brezeanu et al. (2021). Both fine quartz and polymineral grains were mounted on aluminium disks for luminescence measurements.

3.2. Analytical facilities

Luminescence investigations were carried out using a Risø TL-OSL reader (model DA-20) equipped with an automated detection and stimulation head (DASH) (Lapp et al., 2015). The intensity of the blue (470 nm) and infrared (850 nm) LEDs deliver 80 and 300 mW/cm^2, respectively. Luminescence signals were detected by using PDM 9107Q-AP-TTL-03 (160–630 nm) photomultiplier tubes (Thomsen et al., 2006). A 7.5-mm-thick Hoya U-340 UV filter was used for quartz signal determination while the polymineral signals were detected by using a blue filter combination (Schott BG39 + Corning 7–59, with transmission between 320 and 460 nm). A radioactive source of ^{90}Sr–^{90}Y was used for laboratory irradiation. The beta source was calibrated using gamma-irradiated fine (4–11 μm) calibration quartz (Hansen et al., 2015).

The polymineral fine grains aliquots used for residual dose and dose recovery measurements were exposed to window light under natural conditions in order to remove the natural signal.

ESR measurements were performed on an X band Bruker EMX Plus Spectrometer. All samples were placed in quartz glass tubes filled by maintaining the same volume, with a mass between 100 and 200 mg, and the measurements were normalized to 100 mg for inter-comparison. Each sample was measured 3 times and rotated in the cavity between the measurements. Exposure of samples to sunlight during measurements was restricted to a minimum. Measurements were carried out at 90 K (in liquid nitrogen) for Al-h and Ti centres, and at room temperature for E′ and "peroxy" centres. Al-h and "peroxy" spectra were acquired using the following settings: 3350 ± 200 G scanned magnetic field, modulation amplitude 1 G, modulation frequency 100 kHz, microwave power 2 mW, conversion time 50 ms, time constant 40 ms. For Ti measurements the settings were: 3490 ± 110 G scanned magnetic field, modulation amplitude 1 G, modulation frequency 100 kHz, microwave power 10.0 mW, conversion time 10 ms, time constant 20.48 ms, and 10 scans per measurement. For E′ spectra the settings were: 3363 ± 10 G scanned magnetic field, modulation amplitude 0.1 G, modulation frequency 100 kHz, microwave power 0.02 mW, conversion time 30 ms, time constant 20.48 ms, and 3 scans per measurement. Baseline correction was performed using Bruker's Xenon software.

3.3. Equivalent dose determination

Quartz equivalent dose determination has been carried out by using

the standard Single Aliquot Regenerative dose (SAR) protocol (Murray and Wintle 2000, 2003) whereas polymineral fine grains equivalent doses were measured by applying two elevated temperature post-infrared infrared stimulation protocols, namely $pIRIR_{225}$ (Roberts 2008; Buylaert et al., 2009) and $pIRIR_{290}$ (Buylaert et al., 2011a; Thiel et al., 2011). The protocols are outlined in Table S1.

For quartz measurements optical stimulation has been performed using blue-light emitting diodes for 40 s at 125 °C. The net continuous wave optically stimulated luminescence (CW-OSL) signal was integrated over the first 0.308 s of the decay curve minus an early background subtraction in order to reduce the influence of medium and slow components (Cunningham and Wallinga, 2010). A test dose of 17 Gy was used for sensitivity change correction. Thermal treatments consisted of a preheat temperature of 220 °C for 10 s and a cutheat of 180 °C. A high temperature bleach (280 °C for 40 s) was performed at the end of each SAR cycle. In order to assess the robustness of the SAR protocol, the intrinsic performance tests (recycling and recuperation) (Murray and Wintle 2003) were integrated in every measurement. The purity of quartz luminescence signals was checked through the IR depletion test, where an IR stimulation step was added prior to OSL measurement in the last cycle of the SAR protocol (Duller 2003). Only the aliquots with recycling and IR depletion ratios within 10% deviation from unity were considered suitable and used for equivalent dose determination. Recuperation ratios less than 2% of the natural signal were considered acceptable.

Further analysis consisted of equivalent dose determination on polymineral fine grains using two elevated temperature post-infrared infrared stimulation protocols based on a SAR procedure namely $pIRIR_{225}$ (Roberts 2008; Buylaert et al., 2009) (Table S1b) and $pIRIR_{290}$ (Buylaert et al., 2011; Thiel et al., 2011) (Table S1c). A thermal preheat of 250 °C ($pIRIR_{225}$) or 325 °C ($pIRIR_{290}$) was incorporated prior to IR stimulation in every SAR cycle. After the heating step, an IR stimulation at 50 °C for 200 s was performed in order to minimise the charge that is susceptible to fading. The signal of interest was recorded as a result of IR stimulation at a temperature of 225 °C ($pIRIR_{225}$) and 290 °C ($pIRIR_{290}$), respectively. At the end of each measurement cycle a high-temperature bleach for 100 s at 290 °C ($pIRIR_{225}$) and 325 °C ($pIRIR_{290}$) was involved. Sensitivity change corrections have been made by employing a test dose of 17 Gy unless otherwise stated.

3.4. Dosimetry

High-resolution gamma spectrometry was used for the determination of specific radionuclide activities, using a well-type HPGe detector. In order to reach the equilibrium of ^{222}Rn with its parent ^{226}Ra, samples were stored for 1 month before measurements. The annual dose rates were derived following the conversion factors tabulated by Guérin et al. (2011). An alpha efficiency factor of 0.04 ± 0.02 was taken into account for 4–11 μm quartz while for the polymineral fine grains the assumed alpha efficiency value was 0.08 ± 0.02 (Rees-Jones, 1995). These values are consistent with the latter determined efficiency factors of 0.035 ± 0.003 determined by Lai et al. (2008) for 4–11 μm quartz as well as the polymineral fine grains efficiency factors of 0.10 ± 0.014 determined by Schmidt et al. (2018) for pIRIR290 and 0.11 ± 0.02 for pIRIR225 protocol (Kreutzer et al., 2014), respectively. The time averaged water content was assumed to be 15% with a relative error of 25%. The water content was chosen to represent the mean value of the sediment moisture over the entire depositional history. Similar values were used for dating sediments from Canterbury Plains and Banks Peninsula, respectively (Rowan et al., 2012; Sohbati et al., 2016; Brezeanu et al., 2021). The cosmic dose rate was estimated as function of depth, altitude and geomagnetic latitude using the formula proposed by Prescott and Hutton (1994). Given the size of fine grains (4–11 μm), any dose rate derived from internal alpha activity was assumed to be negligible. The specific radionuclide activities and annual doses are presented in Table 1.

4. Results and discussion

4.1. Luminescence properties – quartz

Equivalent doses on fine quartz were determined by interpolating the sensitivity corrected natural OSL signal onto the dose response curve. Fig. 1 shows a representative SAR growth curve and OSL decay curves for a single aliquot of fine quartz extracted from sample NZ 7. The natural and regenerative OSL signal exhibits a similar pattern to the decay measured for calibration quartz during the first seconds of stimulation, which is accepted as being dominated by the fast component (Hansen et al., 2015). The dose response curve was best described by a sum of two saturating exponential functions. Recycling and IR depletion ratios were within 10% deviation from unity which demonstrates that sensitivity corrections are properly made and the quartz signals are pure. Recuperation ratio was less than 2% indicating that the growth curves pass very close to the origin and thermal transfer during the repeated SAR cycle is negligible.

4.1.1. Preheat plateau

The dependency of the equivalent doses on the preheat temperature was investigated through the preheat plateau test. Sample NZ 7 was divided in sets of five aliquots. For each set, a preheat temperature ranging from 180 to 280 °C was applied. A test dose cutheat of 180 °C was employed throughout the measurements. As can be seen from Fig. S2, the equivalent doses do not display any significant variation over the investigated interval of preheat temperatures. The results of the intrinsic SAR tests were satisfactory for all the aliquots measured.

4.1.2. Dose recovery test

Further, a dose recovery test has been performed on six samples (NZ 6, NZ 7, NZ 8, NZ 9, NZ 10 and NZ 11) in order to investigate whether the SAR protocol can successfully determine a known laboratory dose given prior to any thermal treatment (Murray and Wintle, 2003). Sets of five aliquots from each sample were used. The natural signals were bleached by a repeated exposure to blue LEDs for 100 s at room temperature with a pause of 10 ks? The aliquots were irradiated with a beta dose chosen to approximate the natural dose and measured by using the SAR protocol in the same manner as measuring the equivalent dose. Fig. S3 represents the results of the dose recovery test. As can be seen, the dose recovery results for all samples documented here were satisfactory indicating that the SAR protocol can successfully recover laboratory doses up to 46 Gy.

4.1.3. Equivalent doses

The measured quartz equivalent doses are summarized in Table 1. The OSL equivalent doses range from 1.3 ± 0.1 Gy obtained for sample NZ 6 collected from a depth of 10 cm–46 ± 1 Gy for sample NZ 11 which was collected from a depth of 109 cm.

4.2. Luminescence properties – polymineral fine grains

Equivalent doses measured on polymineral fine grains were determined by interpolating the natural sensitivity corrected IRSL signal onto the dose response curve constructed for each sample using both pIRIR protocols. Fig. 2 displays a representative growth curve of sample NZ 7 constructed by applying $pIRIR_{225}$ (Fig. 2a) and $pIRIR_{290}$ (Fig. 2b) protocols, respectively. A comparison between the decay curve of the natural signal and the pattern of a regenerative signal is shown in the insets of Fig. 2. The dose response curves constructed using both pIRIR protocols were best fitted using a sum of two saturating exponential functions. The measured equivalent doses obtained on $pIRIR_{225}$ protocol range from 7.5 ± 0.5 Gy for the youngest sample NZ 6 to 79 ± 2 Gy for sample NZ 10. On the other hand, $pIRIR_{290}$ equivalent doses vary between 23 ± 2 Gy for sample NZ 6 and 121 ± 5 Gy for sample NZ10. As previous studies report a possible influence of the magnitude of the test dose on the $pIRIR_{290}$ laboratory growth curves (Yi et al., 2016; Colarossi

Table 1
Summary of the SAR-OSL, $pIRIR_{225}$ and $pIRIR_{290}$ luminescence ages. The age uncertainties were determined following Aitken and Alldred (1972). The uncertainties associated with the luminescence and dosimetry data are random; the uncertainties mentioned on the optical ages are the overall uncertainties. The systematic errors taken into account include: 2% beta source calibration, 3% conversion factors, 5% attenuation and etching factors, 3% gamma spectrometer calibration, 15% cosmic radiation, 25% water content. All uncertainties represent 1σ. Specific activities were measured using gamma spectrometry and the ages were determined considering 15% water content; adopted alpha efficiency factor was 0.04 ± 0.02 for 4–11 μm quartz and 0.08 ± 0.02 for polymineral 4–11 μm fine grains, respectively (Rees-Jones, 1995). The contribution of cosmic radiation was taken into account and calculated accordingly to Prescott and Hutton (1994). Equivalent doses presented in this table are not corrected for residuals. Equivalent doses presented *in italic* for NZ 8 and NZ 12 pIRIR290 were determined using a test dose of 50 Gy, amounting to about 50% of the equivalent dose. n represents the number of accepted aliquots out of the total number of aliquots measured The measured residual was taken into account for calculation of pIRIR ages, while pIRIR ages calculated using modern analogue correction are denoted by (*). For the sake of completeness IR_{50} ages (uncorrected and corrected for fading) were calculated based on the signals collected during the $pIRIR_{225}$ protocol. g_{2days} values for IR_{50} were measured for samples NZ7, NZ9 and NZ11 and assumed to be 3%/decade in the case of the rest of the samples.

Sample code	Depth (cm)	Equivalent dose (Gy)			Radionuclide concentration (Bq/kg)			Annual dose (Gy/ka)			Age (ka)			Age (ka) (MA) *			
		4–11 μm quartz	$pIRIR_{225}$ pfg	$pIRIR_{290}$ pfg	Ra-226	Th-232	K-40	4–11 μm quartz	$pIRIR_{225}$ pfg	$pIRIR_{290}$ pfg	4–11 μm quartz	$pIRIR_{225}$ pfg	$pIRIR_{290}$ pfg	$pIRIR_{225}$ pfg	$pIRIR_{290}$ pfg	IR_{50} pfg no fading correction	IR_{50} pfg fading corrected
NZ 6	10	1.3 ± 0.1 n = 9/10	7.5 ± 0.5 n = 10/10	23 ± 2 n = 9/10	42 ± 2	48 ± 2	607 ± 17	4.1 ± 0.07	4.6 ± 0.07	4.6 ± 0.07	0.3 ± 0.04	1.2 ± 0.2	4 ± 0.5				
NZ 7	30	26 ± 0.3 n = 14/14	72 ± 1 n = 10/10	111 ± 5 n = 9/10	50 ± 2	42 ± 1	604 ± 16	4.0 ± 0.06	4.5 ± 0.07	4.5 ± 0.07	6.3 ± 0.6	15 ± 1	23 ± 2	14 ± 1	20 ± 2	6.8 ± 0.6	9.1 ± 0.9
NZ 8	50	32 ± 2 n = 7/10	72 ± 1 n = 10/10	114 ± 5 n = 10/10 *113 ± 3* *n=10/10*	38 ± 2	30 ± 1	567 ± 17	2.9 ± 0.05	3.7 ± 0.07	3.7 ± 0.07	11 ± 1	19 ± 2	29 ± 3	17 ± 2	24 ± 2	12 ± 1	16 ± 2
NZ 9	67	39 ± 3 n = 8/10	63 ± 1 n = 10/10	107 ± 6 n = 10/10	29 ± 0.2	22 ± 1	524 ± 14	2.9 ± 0.05	3.1 ± 0.05	3.1 ± 0.05	13 ± 2	19 ± 2	32 ± 3	18 ± 2	27 ± 3	10 ± 1	12 ± 1
NZ 10	85	43 ± 1 n = 10/10	79 ± 2 n = 10/10	121 ± 5 n = 10/10	47 ± 3	30 ± 1	535 ± 13	3.5 ± 0.07	3.9 ± 0.08	3.9 ± 0.08	12 ± 1	20 ± 2	30 ± 3	19 ± 2	26 ± 3	16 ± 1	20 ± 2
NZ 11	109	46 ± 1 n = 10/10	71 ± 1 n = 10/10	90 ± 2 n = 10/10	41 ± 1	26 ± 2	443 ± 14	3.0 ± 0.06	3.3 ± 0.07	3.3 ± 0.07	16 ± 1	21 ± 2	26 ± 2	19 ± 2	20 ± 2	15 ± 1	20 ± 2
NZ 12	129	41 ± 2 n = 10/10	70 ± 1 n = 10/10	99 ± 4 n = 10/10 *103 ± 3* *n=10/10*	34 ± 1	27 ± 2	485 ± 13	3.0 ± 0.05	3.3 ± 0.05	3.3 ± 0.05	14 ± 1	21 ± 2	29 ± 3	19 ± 2	23 ± 2	12 ± 1	15 ± 2

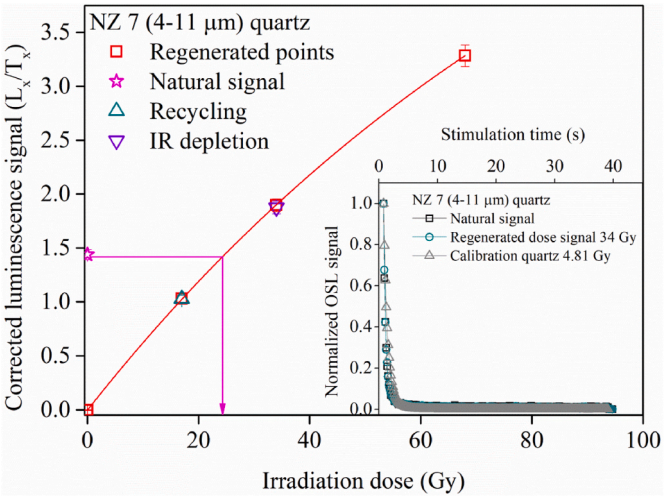

Fig. 1. Representative sensitivity-corrected dose response curve constructed for one aliquot of sample NZ 7 on 4–11 μm quartz using SAR-OSL protocol. The sensitivity corrected natural signals (stars) are interpolated on the dose response curves. IR depletion point is presented as an up triangle while the recycling points are presented as inverse triangles. The inset shows the pattern of a typical quartz decay curve which is compared with the decay of a regenerative dose as well as with the OSL decay of calibration quartz.

et al., 2018) we have additionally investigated the effect of using a test dose with a magnitude of 50% of the equivalent doses (50 Gy) for two samples (NZ 8 and NZ 12). The results obtained are presented in Table 1 and are indistinguishable from the values obtained by using a test dose of 17 Gy pIRIR measured equivalent doses for each sample investigated here are labelled in Table 1.

4.2.1. Residual doses

It is well known that pIRIR signals are more difficult to reset than OSL signals (e.g., Buylaert et al., 2009, 2012; Thiel et al., 2011). Many studies reported residual doses of a few Grays obtained even after long exposure of the aliquots to sunlight or solar simulator (e.g., Buylaert et al., 2011a, 2012; Stevens et al., 2011; Murray et al., 2012; Yi et al., 2016, 2018; Avram et al., 2020, 2022; Brezeanu et al., 2021). Moreover, from long-term bleaching experiments using $pIRIR_{290}$ protocol Yi et al. (2016, 2018) reported that for $pIRIR_{290}$ protocol, a constant residual dose of ~6 ± 1 Gy and ~4 ± 1 Gy is achieved after 300 h beaching in solar simulator for samples collected from Chinese loess. Based on the aforementioned information, the residual dose corrections should be cautiously evaluated especially when dealing with young samples.

The assessment of the residual level has been made on five aliquots of each sample. The natural signal has been erased by exposing the aliquots to sunlight for 30 days prior to measurements. Residual doses obtained using $pIRIR_{225}$ protocol range from 2.1 ± 0.4 Gy for the youngest sample with a measured equivalent dose of 7.5 ± 0.5 Gy to 3.2 ± 0.3 Gy for a sample with a measured equivalent dose of 63 ± 1 Gy. On the other hand, the $pIRIR_{290}$ residual doses vary from 4 ± 1 Gy for the youngest sample with a measured equivalent dose of 23 ± 2 Gy to 6.5 ± 1 Gy for a sample with a measured equivalent dose of 107 ± 6 Gy. The values obtained on each sample are displayed in Table S2. Similar values of residual dose were obtained by Brezeanu et al. (2021) for samples with comparable measured equivalent doses of ~84 Gy and ~120 Gy, respectively. In their study, Brezeanu et al. (2021) reported that a constant residual dose of ~4 ± 1 Gy has been reached after 48 h exposure to sunlight for $pIRIR_{225}$ protocol while in the case of $pIRIR_{290}$ protocol, a constant level of ~10 ± 1 Gy was achieved after 96 h of bleaching for New Zealand loess. They mentioned that such values are in line with those measured after a 30 days exposure to sunlight.

Since it is still questionable whether the natural bleaching condition can be thoroughly replicated in laboratory, it is advisable to use a modern analogue sample for residual dose corrections, as well. In this case, the NZ 6 sample was used as a modern sample. As such, an equivalent dose of 7.5 ± 0.5 Gy was measured using $pIRIR_{225}$ protocol and 22.8 ± 1.5 Gy using $pIRIR_{290}$ protocol, respectively. Based on the laboratory residuals, we considered these values as the maximum residual doses. Thus, the residual dose correction for age calculation was performed by using both laboratory and modern analogue doses (Table 1).

4.2.2. Dose recovery test

The reliability of the measurement protocols was achieved through a dose recovery test (Murray 1996; Wallinga et al., 2000) on five aliquots from samples NZ 6, NZ 7 and NZ 8. The natural signals were removed by exposing the aliquots to window light for 30 days in order to reach a residual level as described in the previous section. Then, the aliquots were irradiated with known laboratory doses that were chosen to approximate the measured equivalent dose. To quantify the accuracy of the protocols to measure laboratory given doses, a ratio between the recovered dose, corrected for the measured residual value and the laboratory given dose was calculated. The results of the dose recovery tests

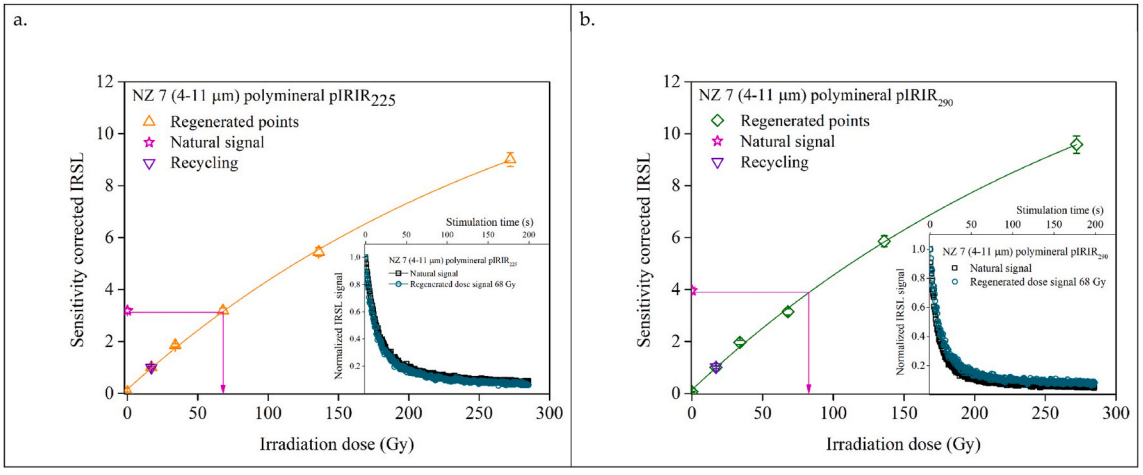

Fig. 2. Representative sensitivity-corrected dose response curves constructed for one aliquot of sample NZ 7 on (a) 4–11 μm polymineral fine grains using the $pIRIR_{225}$ protocol and (b) 4–11 μm polymineral using $pIRIR_{290}$ protocol. The sensitivity corrected natural signals (stars) are interpolated on the dose response curves. The recycling points are presented as inverse triangles. Insets show typical decay curves. For polymineral fine grains, the natural CW-OSL signals are compared to regenerated signals induced by a beta dose approximately equal to the equivalent dose.

for both pIRIR protocols are showed in Fig. 3. As it can be seen, dose recovery ratios obtained for $pIRIR_{225}$ protocol range from 0.98 ± 0.02 for sample NZ 7 to 1.01 ± 0.06 for sample NZ 6 while the $pIRIR_{290}$ protocol dose recovery ratios vary from 1.07 ± 0.06 obtained for sample NZ 6 to 1.23 ± 0.05 calculated for sample NZ 8. These results showed that $pIRIR_{225}$ protocol can successfully recover known doses over the dose interval investigated here, while for $pIRIR_{290}$ protocol some degree of overestimation is observed for doses as large as about 100 Gy. A recent study conducted by Avram et al. (2022) showed that $pIRIR_{290}$ dose recovery ratios overestimate unity between 12% and 46% for given doses that range from ~100 Gy to ~850 Gy.

Some previous studies attributed the poor results of the $pIRIR_{290}$ dose recovery test to the incorrect measurement of the residual dose (e.g., Thomsen et al., 2008; Buylaert et al., 2012). In order to circumvent the potential contribution due to inaccurate estimation for residual doses, a dose recovery test can be carried out by adding laboratory beta doses on top of the natural dose. As such, dose recovery test results are further determined as a ratio between the measured dose and the sum of the natural and additional irradiated dose (equivalent dose + given dose on top) (Buylaert et al., 2011b; Yi et al., 2018).

In this study, five aliquots from samples NZ 6 (measured De = 23 ± 2 Gy), NZ 7 (measured De = 111 ± 5 Gy), NZ 8 (measured De = 114 ± 5 Gy) and NZ 9 (measured De = 107 ± 6 Gy) were irradiated on top of the natural signal with a beta dose of 100 Gy. The results for each the measured dose, corrected using the equivalent dose for all samples are represented in Fig. 3. These results confirm our previous observation that in the case of $pIRIR_{290}$ protocol, a dose overestimation occurs in this dose range.

4.2.3. Fading

Feldspars are known to suffer from anomalous fading phenomenon (Wintle 1973; Spooner 1992, 1994), which is described as the luminescence signal loss under ambient temperature. The percentage of the signal that was lost over a decade can be quantified in term of fading rates (Aitken 1985).

The $pIRIR_{290}$ natural signal is considered to be a stable signal since Thiel et al. (2011) reported for the first time that the natural $pIRIR_{290}$ signal for an old sample is in saturation and thus the ages do not need any further fading corrections. Later, these findings were confirmed by other studies (e.g., Stevens et al., 2011; Buylaert et al., 2011a; Thomsen et al., 2011; Veres et al., 2018). Based on extensive investigations carried out on fading rates of pIRIR signals of polymineral fine grains from loess in Serbia (Avram et al., 2020), as well as based on the very low values obtained for the fading rates of $pIRIR_{225}$ signals of polymineral fine grains form loess at a nearby site in New Zealand (Brezeanu et al., 2021), we have tested for fading only the $pIRIR_{225}$ signals here. Five aliquots from sample NZ 7, NZ 9 and NZ 11 were used in this respect. These aliquots were previously used for a dose recovery test. A beta dose of 100 Gy was used in the experiment, while the test dose magnitude was kept as in the equivalent dose measurements. To test the reproducibility of the measurements four consecutive prompt reads-out were applied prior to delayed measurements. A preheat treatment was included prior to storage. Storage time ranging between 2 h and 2 days were used. The results of the fading test are presented in Table S3. For all samples, the variation of the measured fading rates obtained on different aliquots is small. For sample NZ 7 a g-value of 1.06 ± 0.16%/decade was measured whereas for sample NZ 11 the average measured fading rate was 1.03 ± 0.28. On the other hand, a negative fading rate value of −0.04 ± 0.03 was measured for sample NZ 9. Such low values for the fading rates are considered to be laboratory artefact (Vasiliniuc et al., 2012) and the $pIRIR_{225}$ ages do not need any correction for fading (Avram et al., 2020, 2022; Brezeanu et al., 2021). Therefore, in the further sections are discussed the uncorrected pIRIR ages.

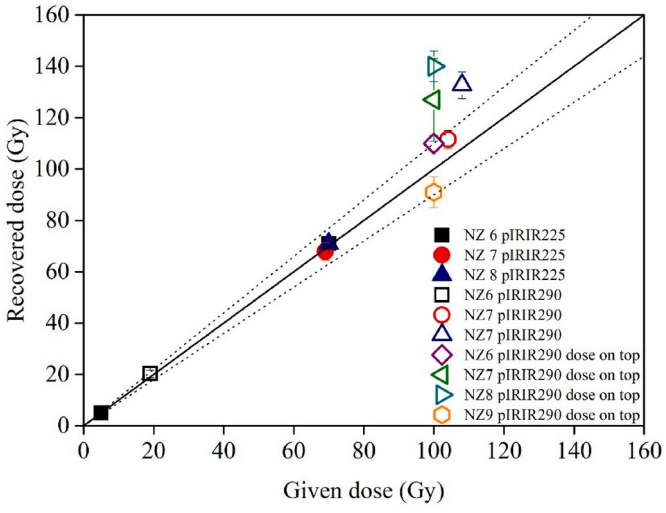

Fig. 3. The results of dose recovery test using $pIRIR_{225}$ protocol and $pIRIR_{290}$ protocol on 4–11 μm polymineral aliquots from sample NZ 6, NZ 7 and NZ 8. Dose recovery test result when 100 Gy was added on top of the natural accrued dosed of samples NZ 6, NZ 7, NZ 8 and NZ 9 are also depicted. Five aliquots were used for each datapoint. The solid line represents y(x) = x function while the dotted line represent 10% deviation from this dependence.

4.3. ESR investigations

As the poor luminescence properties of coarse quartz in the region are well known (Preusser et al., 2006) and were characterised in detail at a nearby site (Brezeanu et al., 2021), it is important to gain a better understanding of the intrinsic and extrinsic defects that exist in the fine fraction compared to the coarser fractions given that it was shown above that the first is amenable to the application of OSL dating, contrary to the latter. In this respect, ESR analysis have been performed on different grain sizes of quartz (4–11 μm, 63–90 μm, 90–125 μm, 125–180 μm and 180–250 μm) extracted from sample NZ 3 which was collected from the nearby loess profile investigated by Brezeanu et al. (2021), as this was the only sample from which sufficient amount of quartz of different grain sizes could be extracted for analysis. In view of the proximity of the sites (less than 1 km apart, see Fig. S1), the sedimentary sequences are expected to be similar. This is confirmed by geological mapping carried out at the sites and in between, which confirms identical outcrops (Micallef et al., 2021). At such it is reasonable to assume that the source rocks of the sedimentary material at both sites are similar. Luminescence properties of coarser fractions of quartz were thoroughly described in Brezeanu et al. (2021) while 4–11 μm quartz fraction of sample NZ 3 presents similar luminescence characteristics as those displayed by the investigated samples from this study (NZ 6-NZ 12), and an equivalent dose of 29 ± 3 Gy was determined by measuring 8 aliquots.

Fig. 4 presents the ESR spectra of the different grain sizes of quartz compared to calibration quartz, a 180–250 μm quartz fraction separated from aeolian sand from Rømø, Jutland, Denmark, provided by Risø National Laboratory (Hansen et al., 2015) and investigated by ESR in Timar-Gabor (2018). No significant differences regarding the presence of paramagnetic species were observed between the investigated NZ3 sample and the calibration quartz.

The intensities of ESR signals were given in Table 2. The intensity of Al-h signal was determined from peak-to-peak amplitude measurements between the top of the first peak (g = 2.018) to the bottom of the last peak (g = 1.993) (Toyoda and Falguères, 2003). For the Ti centre the intensities were obtained using "options A, B and D" described in Duval and Guilarte (2015) and Duval et al. (2017), associated with a mixture of Ti–H and Ti–Li centres. Option A was measured from the top of g = 1.979 to the bottom of the peak around g = 1.913–1.915, option B as a peak-to-peak amplitude of the signal at g = 1.931 and option D as a peak-to-baseline amplitude of the signal g = 1.913–1.915. The intensity of the E' signal was evaluated from the peak-to-peak height of the signal,

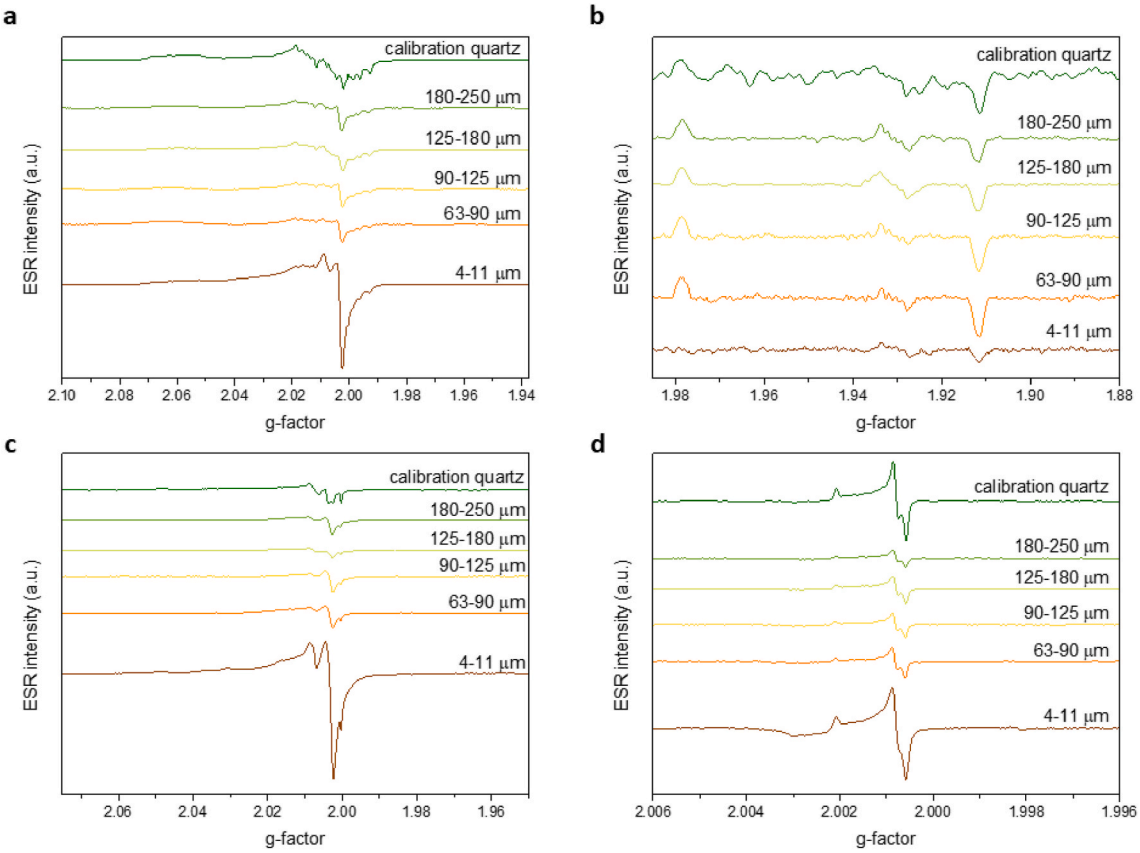

Fig. 4. ESR spectra of Al-h (a), Ti (b), "peroxy"(c), and E′(d) centres, for quartz fractions 4–11, 63–90, 90–125, 125–180, 180–250 μm from sample NZ 3, and for calibration quartz.

Table 2
ESR signal intensities of Al-h, Ti (option A, B, D), "peroxy", and E' centres, for fractions 4–11, 63–90, 90–125, 125–180, 180–250 μm and calibration quartz.

Sample	Al	st err	Ti A	st err	Ti B	st err	Ti D	st err	peroxy	st err	E′	st err
4–11 μm	1.5939	0.0056	0.0769	0.0112	0.0429	0.0080	0.0610	0.0070	2.2026	0.0099	0.4766	0.0073
63–90 μm	0.5596	0.0041	0.2141	0.0047	0.0687	0.0067	0.1295	0.0045	0.5018	0.0102	0.1571	0.0062
90–125 μm	0.5641	0.0082	0.1778	0.0104	0.0611	0.0072	0.1143	0.0094	0.4660	0.0016	0.1317	0.0020
125–180 μm	0.7602	0.0073	0.1557	0.0028	0.0842	0.0065	0.0966	0.0033	0.4569	0.0053	0.1430	0.0008
180–250 μm	0.7250	0.0105	0.1304	0.0222	0.0934	0.0005	0.0774	0.0117	0.4598	0.0093	0.0943	0.0030
Calibration quartz	1.7286	0.0158	0.0968	0.0028	0.0598	0.0040	0.0576	0.0024	0.5107	0.0132	0.4435	0.0196

and for "peroxy" signal it was determined from the peak-to-peak height from g ≈ 2.003 to g ≈ 2.009 (Odom and Rink, 1989).

ESR spectra of Al-h centre (Fig. 4a) show a significant contribution from the "peroxy" signal, which is relatively strong in these samples (Fig. 4c). Al-h and "peroxy" signals are considerably stronger in 4–11 μm quartz, compared to other fractions, about 3 and 4 times higher than in the case of 63–90 μm fraction, for Al-h and "peroxy" respectively. Interestingly, Ti signals are very weak in all of the investigated samples, especially in the 4–11 μm fraction (Fig. 4b), for which the intensity amounts to 40–60% of the intensity observed for 63–90 μm fraction. E′ signal intensity in the smallest fraction is about 3 times bigger than in 63–90 μm fraction, and reduces with increasing grain size (Fig. 4d). General trends observed in the case of fine grains compared to the coarse ones – a higher intensity of Al-h, "peroxy" and E' signals, as well as very low intensity of Ti centres, are the same as reported in Timar-Gabor (2018) for samples which displayed a very good OSL behaviour (quartz from loess from Roxolany, Ukraine (Anechitei-Deacu et al., 2018) and Stayky, Ukraine (Veres et al., 2018). This suggests that the cause of the poor OSL properties of the investigated coarse grained quartz samples might be connected with some non-paramagnetic species, which cannot be detected by ESR spectroscopy.

5. Luminescence ages

Luminescence ages obtained by using SAR-OSL protocol on fine quartz as well as $pIRIR_{225}$ and $pIRIR_{290}$ protocols, respectively, are presented in Table 1 along with the dosimetry data. Only the pIRIR ages calculated with the modern analogue correction are discussed in this section.

Fine quartz luminescence ages range from 0.3 ± 0.04 ka for sample NZ 6 which was collected from the uppermost part of the section to 13 ± 2 ka for sample NZ 9.

The $pIRIR_{225}$ ages calculated using a residual dose correction based on the modern analogue sample range between 14 ± 1 ka for sample NZ 7 and 18 ± 2 ka for sample NZ 9 for $pIRIR_{225}$ protocol. On the other hand, luminescence ages measured using $pIRIR_{290}$ protocol, using the same residual correction vary from 20 ± 2 ka for sample NZ 7 to 27 ± 3 ka for sample NZ 9. As can be seen, the $pIRIR_{290}$ luminescence ages are slightly higher than those measured using $pIRIR2_{225}$ protocol. Such age discrepancy between the two pIRIR protocols over this age interval has been previously observed in several studies, such as on European loess (Zhang et al., 2018; Avram et al., 2020) and on New Zealand loess (Micallef et al., 2021; Brezeanu et al., 2021), respectively.

The two sets of pIRIR ages calculated based on modern analogue correction along with the fine quartz SAR-OSL ages are presented in Fig. S4 as function of depth. An age reversal can be observed between sample NZ 9 and NZ 10, and occur between a depth of ~70 cm and ~130 cm. Such age reversal has been previously observed at the same depths from a nearby loess site by Brezeanu et al. (2021) as well as by others in the Canterbury region (e.g., Berger et al., 2001; Almond et al., 2007; Rowan et al., 2012).

As can be seen from Fig. S4, an age discrepancy between the three sets of ages is displayed. Based on dose recovery test results as well as on the previous findings (e.g., Veres et al., 2018; Constantin et al., 2019; Avram et al., 2020, 2022), we interpret the $pIRIR_{290}$ ages as being overestimated. Moreover, the SAR-OSL fine quartz and $pIRIR_{225}$ ages are not in agreement even though the behaviour in the SAR procedure was satisfactory for both minerals. The $pIRIR_{225}$ age for sample NZ 7 (14 ± 1 ka) collected from a depth of 30 cm is similar with that obtained by Brezeanu et al. (2021) for sample NZ 2 (14 ± 1 ka) which was collected from the same depth. Such overlapping was also found for samples collected from a depth of ~50 and ~130 cm, respectively. As there is evidence that reliable age up to ~50 ka can be obtained on fine quartz (e.g., Timar-Gabor and Wintle 2013; Avram et al., 2020), the differences between the OSL and $pIRIR_{225}$ ages reported here require further investigations. IR_{50} ages estimated based on signals collected during the application of the $pIRIR_{225}$ protocol support this conclusion.

6. Summary and conclusions

In this study the SAR-OSL protocol has been applied for the first time on fine quartz alongside $pIRIR_{225}$ and $pIRIR_{290}$ protocols on polymineral fine grains for dating seven samples of loess from an exposure in Southern Canterbury Plains South Island of New Zealand. Luminescence behaviour of fine quartz in the SAR procedure was investigated in the regard of IR depletion test, preheat plateau test and dose recovery tests, respectively. The satisfactory results that have been obtained for all the investigated tests have led to obtaining for the first-time fine quartz luminescence ages for the investigated loess profile. Moreover, two sets of pIRIR ages have been also determined on polymineral fine grains extracted from the same samples. All three sets of ages range up to 13 ± 2 ka (fine quartz), 18 ± 2 ka ($pIRIR_{225}$) and 27 ± 3 ka ($pIRIR_{290}$), respectively suggesting that loess from the investigated profile was accumulated during the last glacial maximum. As coarse quartz fractions were not amenable for OSL dating ESR investigations were performed on different grain sizes of quartz. The main ESR impurity defects (Al and Ti centres) as well as the most dominant intrinsic defects (E′ and "peroxy") showed trends similar to those previously reported for samples characterised by a very good OSL behaviour, namely a higher intensity of Al-h, "peroxy" and E' signals, and much lower intensity of Ti signals observed in the case of fine grains compared to the coarse grains. The lack of significant differences in ESR signals between the samples suitable for OSL dating such as calibration quartz and other samples previously investigated and the New Zealand samples which display a poor luminescence behaviour suggest that the factors leading to the different OSL characteristics might be connected with some non-paramagnetic species, which cannot be detected by ESR spectroscopy.

Declaration of competing interest

The authors declare that they have no known competing financial interests or personal relationship that could have appeared to influence the work reported in this paper.

Acknowledgements

This study was funded by the European Research Council (ERC) under the European Union's Horizon 2020 research and innovation programme ERC-2015-STG (grant agreement No [678106]).

A. Avram and A. Timar-Gabor acknowledge the financial support of the research project EEA-RO–NO–2018-0126.

A. Micallef acknowledges the financial support from the European Research Council (ERC) under the European Union's Horizon 2020 research and innovation programme (grant MARCAN 677898).

Appendix A. Supplementary data

Supplementary data to this article can be found online at https://doi.org/10.1016/j.radmeas.2022.106788.

References

Aitken, M.J., Alldred, J.C., 1972. The assessment of error limits in thermoluminescent dating. Archaeometry 14, 257–267.

Aitken, M.J., 1985. Thermoluminescence Dating. Academic Press, London, p. 360.

Alloway, B.V., Lowe, D.J., Barrell, D.J.A., Newnham, R.M., Almond, P.C., Augustinus, P. C., Bertler, N.A.N., Carter, L., Litchfield, N.J., McGlone, M.S., Shulmeister, J., Vandergoes, M., Williams, P., NZ-INTIMATE Members, 2007. Towards a climate event stratigraphy for New Zealand over the past 30 000 years (NZ-INTIMATE project). J. Quat. Sci. 22 (1), 9–35. https://onlinelibrary.wiley.com/doi/abs/10.1002/jqs.1079.

Almond, P.C., Moar, N.T., Lian, O.B., 2001. Reinterpretation of the glacial chronology of South Westland, New Zealand. N. Z. J. Geol. Geophys. 44, 1–15. https://doi.org/10.1080/00288306.2001.9514917.

Almond, P.C., Shanhun, F.L., Rieser, U., Shulmeister, J., 2007. An OSL, radiocarbon and tephra isochron-based chronology for birdlings flat loess at Ahuriri Quarry, Banks Peninsula, Canterbury, New Zealand. Quateranary Geochronology 2, 4–8. https://doi.org/10.1016/j.quageo.2006.06.002.

Anechitei-Deacu, V., Timar-Gabor, A., Constantin, D., Trandafir-Anothi, O., Del Valle, L., Fornos, J.J., Gomez-Pujol, L., Wintle, A.G., 2018. Assessing the maximum limit of SAR-OSL dating using quartz of different grain sizes. Geochronometria 45, 146–159. https://doi.org/10.1515/geochr-2015-0092.

Avram, A., Constantin, D., Veres, D., Kelemen, S., Obreht, I., Hambach, U., Marković, S. B., Timar-Gabor, A., 2020. Testing polymineral post-IR IRSL and quartz SAR-OSL protocols on Middle to Late Pleistocene loess at Batajnica, Serbia. Boreas 49, 615–663. https://onlinelibrary.wiley.com/doi/full/10.1111/bor.12442.

Avram, A., Constantin, D., Hao, Q., Timar-Gabor, A., 2022. Optically stimulated luminescence dating of loess in South-Eastern China using quartz and polymineral fine grains. Quat. Geochronol. 67, 101226 https://doi.org/10.1016/j.quageo.2021.101226.

Berger, G.W., Pillans, B.J., Tonkin, P.J., 2001. Luminescence chronology of loess-paleosol sequences from Canterbury, South Island, New Zealand. N. Z. J. Geol. Geophys. 44, 501–516. https://doi.org/10.1080/00288306.2001.9514952.

Berger, G.W., Pillans, B.J., Bruce, J.G., McIntosh, P.D., 2002. Luminescence chronology of loess-paleosol sequences from southern South Island, New Zealand. Quat. Sci. Rev. 21, 1899–1913. https://doi.org/10.1016/S0277-3791(02)00021-5.

Bösken, J., Klasen, N., Zeeden, C., Obreht, I., Marković, S.B., Hambach, U., Lehmkuhl, F., 2017. New luminescence-based geochronology framing the last two glacial cycles at the southern limit of European Pleistocene loess in Stalać (Serbia). Geochronometria 44, 150–161. https://doi.org/10.1515/geochr-2015-0062.

Buylaert, J.P., Murray, A.S., Thomsen, K.J., 2009. Testing the potential of an elevated temperature IRSL signal from K-feldspar. Radiat. Meas. 44, 560–565. https://doi.org/10.1016/j.radmeas.2009.02.007.

Buylaert, J.P., Huot, S., Murray, A.S., Van Den Haute, P., 2011a. Infrared stimulated luminescence dating of an Eemian (MIS 5e) site in Denmark using K-feldspar. Boreas 40, 46–56. https://doi.org/10.1111/j.1502-3885.2010.00156.x.

Buylaert, J.P., Thiel, C., Murray, A., Vandenberghe, S., Yi, S., Lu, H., 2011b. IRSL and post-IR IRSL residual doses recorded in modern dust samples from the Chinese loess plateau. Geochronometria 38, 432–440. https://doi.org/10.2478/s13386-011-0047-0.

Buylaert, J.-P., Jain, M., Murray, A.S., Thomsen, K.J., Thiel, C., Sohbati, R., 2012. A robust feldspar luminescence dating method for Middle and Late Pleistocene sediments. Boreas 41, 435–451. https://doi.org/10.1111/j.1502-3885.2012.00248.x.

Brezeanu, D., Avram, A., Micallef, A., CintaPinzaru, S., Timar-Gabor, A., 2021. Investigations on the luminescence properties of quartz and feldspars extracted from loess in the Canterbury Plains, New Zealand South Island. Geochronometria 48, 46–60. https://doi.org/10.2478/geochr-2021-0005.

Colarossi, D., Duller, G.A.T., Roberts, H.M., 2018. Exploring the behaviour of luminescence signals from feldspars: implications for the single aliquot regenerative dose protocol. Radiat. Meas. 109, 35–44. https://doi.org/10.1016/j.radmeas.2017.07.005.

Constantin, D., Veres, D., Panaiotu, C., Anechitei-Deacu, V., Groza, S.M., Begy, R.C., Kelemen, S., Buylaert, J.-P., Hambach, U., Markovic, S.B., Gerasimenko, N., Timar-Gabor, A., 2019. Luminescence age constraints on the Pleistocene-Holocene transition recorded in loess sequences across SE Europe. Quat. Geochronol. 49, 71–77. https://doi.org/10.1016/j.quageo.2018.07.011.

Cunningham, A.C., Wallinga, J., 2010. Selection of integration time intervals for quartz OSL decay curves. Quat. Geochronol. 5, 657–666. https://doi.org/10.1016/j.quageo.2010.08.004.

Duller, G.A.T., 2003. Distinguishing quartz and feldspars in single grain luminescence measurements. Radiat. Meas. 37, 161–165. https://doi.org/10.1016/S1350-4487(02)00170-1.

Duval, M., Guilarte, V., 2015. ESR dosimetry of optically bleached quartz grains extracted from Plio-Quaternary sediment: evaluating some key aspects of the ESR signals associated to the Ti-centers. Radiat. Meas. 78, 28–41. https://doi.org/10.1016/j.radmeas.2014.10.002.

Duval, M., Arnold, L.J., Guilarte, V., Demuro, M., Santonja, M., Pérez-González, A., 2017. Electron spin resonance dating of optically bleached quartz grains from the Middle Palaeolithic site of Cuesta de la Bajada (Spain) using the multiple centres approach. Quat. Geochronol. 37, 82–96. https://doi.org/10.1016/j.quageo.2016.09.006.

Frechen, M., Schweitzer, U., Zander, A., 1996. Improvements in sample preparation for the fine grain technique. Ancient TL 14, 15–17.

Guérin, G., Mercier, N., Adamiec, G., 2011. Dose-rate conversion factors: update. Ancient TL 29, 5–8.

Hansen, V., Murray, A., Buylaert, J.P., Yeo, E.Y., Thomsen, K., 2015. A new irradiated quartz for beta source calibration. Radiat. Meas. 81, 123–127. https://doi.org/10.1016/j.radmeas.2015.02.017.

Hornblow, S., Quigley, M., Nicol, A., Van Dissen, R., Wang, N., 2014. Paleoseismology of the 2010 Mw 7.1 Darfield (Canterbury) earthquake source, Greendale fault, New Zealand. Tectonophysics 637, 178–190. https://doi.org/10.1016/j.tecto.2014.10.004.

Holdaway, R.N., Roberts, R.G., Beavan-Athfield, N.R., Olley, J.M., Worthy, T.H., 2002. Optical dating of quartz sediments and accelerator mass spectrometry 14C dating of bone gelatin and moa eggshell: a comparison of age estimates for non-archaeological deposits in New Zealand. J. Roy. Soc. N. Z. 32, 463–505. https://doi.org/10.1080/03014223.2002.9517705.

Hormes, A., Preusser, F., Denton, G., Hajdas, I., Weiss, D., Stocker, T.F., Schlüchter, C., 2003. Radiocarbon and luminescence dating of overbank deposits in outwash sediments of the Last Glacial Maximum in North Westland, New Zealand. N. Z. J. Geol. Geophys. 46, 95–106. https://doi.org/10.1080/00288306.2003.9514998.

Kreutzer, S., Schmidt, C., DeWitt, R., Fuchs, M., 2014. The a-value of polymineral fine grain samples measured with the post-IR IRSL protocol. Radiat. Meas. 63, 18–29. https://doi.org/10.1016/j.radmeas.2014.04.027.

Lai, Z.P., Zöller, L., Fuchs, M., Brückner, H., 2008. Alpha efficiency determination for OSL of quartz extracted from Chinese loess. Radiat. Meas. 43, 767–770. https://doi.org/10.1016/j.radmeas.2008.01.022.

Lapp, T., Kook, M., Murray, A.S., Thomsen, K.J., Buylaert, J.P., Jain, M., 2015. A new luminescence detection and stimulation head for the Risø TL/OSL reader. Radiat. Meas. 81, 178–184. https://doi.org/10.1016/j.radmeas.2015.02.001.

Lang, A., Lindauer, S., Kuhn, R., Wagner, G.A., 1996. Procedures used for optically and infrared stimulated luminescence dating of sediments in Heidelberg. Ancient TL 14, 7–11.

Micallef, A., Marchis, R., Saadatkhah, N., Pondthai, P., Everett, M.E., Avram, A., Timar-Gabor, A., Cohen, D., Preca Trapani, R., Weymer, B.A., Wernette, P., 2021. Groundwater erosion of coastal gullies along the Canterbury coast (New Zealand): a rapid and episodic process controlled by rainfall intensity and substrate variability. Earth Surf. Dyn. 9, 1–18. https://doi.org/10.5194/esurf-9-1-2021.

Murray, A.S., 1996. Developments in optically stimulated luminescence and photo-transferred thermoluminescence dating of young sediments: application to a 2000-years of flood deposits. Geochem. Cosmochim. Acta 60, 565–576. https://doi.org/10.1016/0016-7037(95)00418-1.

Murray, A.S., Wintle, A.G., 2000. Luminescence dating using an improved single-aliquot regenerative-dose protocol. Radiat. Meas. 32, 57–73. https://doi.org/10.1016/S1350-4487(99)00253-X.

Murray, A.S., Wintle, A.G., 2003. The single aliquot regenerative dose protocol: potential for improvements in reliability. Radiat. Meas. 37, 377–381. https://doi.org/10.1016/S1350-4487(03)00053-2.

Murray, A.S., Thomsen, K.J., Masuda, N., Buylaert, J.P., Jain, M., 2012. Identifying well-bleached quartz using the different bleaching rates of quartz and feldspar luminescence signals. Radiat. Meas. 47, 688–695. https://doi.org/10.1016/j.radmeas.2012.05.006.

Nichol, S.L., Lian, O.B., Carter, C.H., 2003. Sheet-gravel evidence for a late Holocene tsunami run-up on beach dunes, Great Barrier Island, New Zealand. Sediment. Geol. 155, 129–145.

Odom, A.L., Rink, W.J., 1989. Natural accumulation of Schottky-Frenkel defects: implications for a quartz geochronometer. Geology 17 (1), 55–58. https://doi.org/10.1130/0091-7613(1988)017<0055:NAOSFD>2.3.CO;2.

Prescott, J.R., Hutton, J.T., 1994. Cosmic ray contributions to dose rates for luminescence and ESR dating: large depths and long term variations. Radiat. Meas. 23, 497–500. https://doi.org/10.1016/1350-4487(94)90086-8.

Preusser, F., Andersen, B.G., Denton, G.H., Schlüchter, C., 2005. Luminescence chronology of Late Pleistocene glacial deposits in north Westland, New Zealand. Quat. Sci. Rev. 24, 2207–2227. https://doi.org/10.1016/j.quascirev.2004.12.005.

Preusser, F., Ramseyer, K., Schlüchter, C., 2006. Characterisation of low OSL intensity quartz from the New Zealand Alps. Radiat. Meas. 41, 871–877. https://doi.org/10.1016/j.radmeas.2006.04.019.

Rees-Jones, J., 1995. Optical dating of young sediments using fine-grain quartz. Ancient TL 13, 9–13.

Roberts, H., 2008. The development and application of luminescence dating to loess deposits: a perspective on the past, present and future. Boreas 37, 483–507. https://doi.org/10.1111/j.1502-3885.2008.00057.x.

Roberts, H.M., 2015. Luminescence dating, loess. In: Rink, W.J., Thompson, J.W. (Eds.), Encyclopedia of Scientific Dating Methods. Springer, pp. 425–430.

Rowan, A.V., Roberts, H.M., Jones, M.A., Duller, G.A.T., Covey-Crump, S.J., Brocklehurst, S.H., 2012. Optically stimulated luminescence dating of glaciofluvial sediments on the Canterbury Plains, South Island, New Zealand. Quat. Geochronol. 8, 10–22. https://doi.org/10.1016/j.quageo.2011.11.013.

Rother, H., Shulmeister, J., Rieser, U., 2009. Stratigraphy, optical dating chronology (IRSL) and depositional model of pre-LGM glacial deposits in the Hope Valley, New Zealand. Quat. Sci. Rev. 1–17. https://doi.org/10.1016/j.quascirev.2009.11.001.

Schmidt, C., Bösken, J., Kolb, T., 2018. Is there a common alpha-efficiency in polymineral samples measured by various infrared stimulated luminescence protocols? Geochronometria 45, 160–172. https://doi.org/10.1515/geochr-2015-0095.

Shulmeister, J., Thackray, G.D., Rieser, U., Hyatt, O.M., Rother, H., Smart, C.C., Evans, D. J., 2010. The stratigraphy, timing and climatic implications of glaciolacustrine deposits in the middle Rakaia Valley, South Island, New Zealand. Quat. Sci. Rev. 29, 2362–2381. https://doi.org/10.1016/j.quascirev.2010.06.004.

Sohbati, R., Borella, J., Murray, A., Quigley, M., Buylaert, J.P., 2016. Optical dating of loessic hillslope sediments constrains timing of prehistoric rockfall, Christchurch, New Zealand. J. Quat. Sci. 31, 678–690. https://doi.org/10.1002/jqs.2895.

Stevens, T., Marković, S.B., Zech, M., Hambach, U., Sümegi, P., 2011. Dust deposition and climate in the Carpathian Basin over an independently dated last glacial-interglacial cycle. Quat. Sci. Rev. 30, 662–681. https://doi.org/10.1016/j.quascirev.2010.12.011.

Spooner, N.A., 1992. Optical dating—preliminary-results on the anomalous fading of luminescence from feldspars. Quat. Sci. Rev. 11, 139–145. https://doi.org/10.1016/0277-3791(92)90055-D.

Spooner, N.A., 1994. The anomalous fading of infrared-stimulated luminescence from feldspars. Radiat. Meas. 23, 625–632. https://doi.org/10.1016/1350-4487(94)90111-2.

Thiel, C., Buylaert, J.P., Murray, A., Terhorst, B., Hofer, I., Tsukamoto, S., Frechen, M., 2011. Luminescence dating of the Stratzing loess profile (Austria) – testing the potential of an elevated temperature post-IR IRSL protocol. Quat. Int. 234, 23–31. https://doi.org/10.1016/j.quaint.2010.05.018.

Thomsen, K.J., Bøtter-Jensen, L., Denby, P.M., Moska, P., Murray, A.S., 2006. Developments in luminescence measurement techniques. Radiat. Meas. 41, 768–773. https://doi.org/10.1016/j.radmeas.2006.06.010.

Thomsen, K.J., Murray, A.S., Jain, M., 2011. Stability of IRSL signals from sedimentary K-feldspar samples. Geochronometria 38, 1–13. https://doi.org/10.2478/s13386-011-0003-z.

Timar-Gabor, A., Wintle, A.G., 2013. On natural and laboratory generated dose response curves for quartz of different grain sizes from Romanian loess. Quat. Geochronol. 18, 34–40. https://doi.org/10.1016/j.quageo.2013.08.001.

Timar-Gabor, A., 2018. Electron spin resonance characterisation of sedimentary quartz of different grain sizes. Radiat. Meas. 120, 59–65. https://doi.org/10.1016/j.radmeas.2018.06.023.

Toyoda, S., Falguères, C., 2003. The method to represent the ESR signal intensity of the aluminum hole center in quartz for the purpose of dating. Adv. ESR Appl. 20, 7–10.

Veres, D., Tecsa, V., Gerasimenko, N., Zeeden, C., Hambach, U., Timar-Gabor, A., 2018. Short-term soil formation events in last glacial east European loess, evidence from multi-method luminescence dating. Quat. Sci. Rev. 34–51. https://doi.org/10.1016/j.quascirev.2018.09.037, 200.

Vasiliniuc, Ş., Vandenberghe, D.A.G., Timar-Gabor, A., Panaiotu, C., Cosma, C., 2012. Testing the potential of elevated temperature post-IR IRSL signals for dating Romanian loess. Quat. Geochronol. 10, 75–80. https://doi.org/10.1016/j.quageo.2012.02.014.

Wallinga, J., Murray, A., Duller, G., 2000. Underestimation of equivalent dose in single-aliquot optical dating of feldspars caused by preheating. Radiat. Meas. 32, 691–695. https://doi.org/10.1016/S1350-4487(00)00127-X.

Wintle, A.G., 1973. Anomalous fading of thermoluminescence in mineral samples. Nature 245, 143–144. https://doi.org/10.1038/245143a0.

Yi, S., Buylaert, J.P., Murray, A.S., Lu, H., Thiel, C., Zeng, L., 2016. A detailed post-IR IRSL dating study of the Niuyangzigou loess site in northeastern China. Boreas 45, 644–657. https://doi.org/10.1111/bor.12185.

Yi, S., Li, X., Han, Z., Lu, H., Liu, J., Wu, J., 2018. High resolution luminescence chronology for Xiashu Loess deposits of Southern China. J. Asian Earth Sci. 155, 188–197. https://doi.org/10.1016/j.jseaes.2017.11.027.

Yates, K., Fenton, C.H., Bell, D.H., 2018. A review of the geotechnical characteristics of loess and loess-derived soils from Canterbury, South Island, New Zealand. Eng. Geol. 236, 11–21. https://doi.org/10.1016/j.enggeo.2017.08.001.

Zhang, J., Rolf, C., Wacha, L., Tsukamoto, S., Durn, G., Frechen, M., 2018. Luminescence dating and palaeomagnetic age constraint of a last glacial loess-paleosol sequence from Istria, Croatia. Quat. Int. 494, 19–33. https://doi.org/10.1016/j.quaint.2018.05.045.